Geophysica Norvegica

ARNT ELIASSEN AND MAGNE LYSTAD
The Ekman layer of a circular vortex.
A numerical and theoretical study

VOL. 31 NO. 7 . 1977
UNIVERSITETSFORLAGET

GEOPHYSICA NORVEGICA . VOL. 31 . NO. 7 . PAGES 1-16 . 1977
UNIVERSITETSFORLAGET

Geophysica Norvegica

is a journal of geophysics, issued under the auspices of the Norwegian Academy of Science and Letters

PUBLISHER

Universitetsforlaget: P. O. Box 7508, Skillebekk, Oslo 2, Norway
P. O. Box 142, Boston, Mass, 02113, U.S.A.

SUBSCRIPTION

Geophysica Norvegica (Geofysiske Publikasjoner) is published at irregular intervals. Order from the Publisher, Universitetsforlaget.

Geophysica Norvegica (Geofysiske Publikasjoner) is a series of scientific publications issued by the Norwegian Academy of Science and Letters. The Geophysical Commission appoints an editor and editorial committee.
Manuscripts for publication in *Geophysica Norvegica* should be carefully prepared (see Instructions to Author on p. 3 of the cover) and sent to the editor. The next step is the manuscript's submission to the Academy by a competent member, who is responsible for ensuring that the paper meets a sufficiently high scientific standard. (Members of the Academy are allowed to submit their own papers.) The final decision as to whether the paper should be published is taken by the editor.
Geophysica Norvegica is mainly intended as a journal for Norwegian authors, but papers from other authors may be accepted provided that the work has been carried out at a Norwegian institution or its content has a special relevance to Norway.

The Ekman layer of a circular vortex. A numerical and theoretical study

ARNT ELIASSEN
Institute of Geophysics, University of Oslo, Norway

MAGNE LYSTAD
Norwegian Meteorological Institute, Norway

Eliassen, A. & Lystad, M. The Ekman layer of a circular vortex. A numerical and theoretical study. *Geophysica Norvegica*, Vol. 31, No. 7, 1977.

The vortex motion of a homogeneous and incompressible fluid with a constant eddy viscosity, bounded by two parallel, rotating planes is studied. The filtered equations describing the slow evolution of the vortex, with inertia oscillations eliminated, are integrated numerically from an initial state, in which there is a differential rotation between the fluid and the boundary planes. A slip boundary condition is used at the planes, and the structure of the Ekman layers and the spindown process is studied in relation to the value of the drag coefficient and the Rossby number (or overrotation rate) of the initial state. The numerical results are in good agreement with the theoretical results of A. Eliassen (1971).

A. Eliassen, Institute of Geophysics, University of Oslo, P.O. Box 1022, Blindern, Oslo 3, Norway

1. INTRODUCTION

In atmospheric and oceanic vortices, the Ekman boundary layer next to the bottom boundary represents a forcing mechanism for a secondary 'meridional' vertical circulation which extends outside the Ekman layer and produces a change of the vortex strength by advection of angular momentum. Although the Ekman layer is not the only forcing mechanism for such vertical circulations, it is still of interest to study the Ekman layer forcing separately.

The present paper deals with the Ekman layer in a homogeneous and incompressible fluid, where other forcing mechanisms are ruled out. Horizontal momentum is assumed to be diffused vertically by turbulent eddies which give rise to a constant eddy viscosity. Within the fluid, such a turbulent viscosity produces the same effect as molecular viscosity in laminar flow, but the boundary conditions are essentially different in these two cases. In laminar flow, the fluid sticks to the lower boundary. In a turbulent fluid, on the other hand, the constant eddy viscosity cannot be applied all the way down to the lower boundary, where the eddy viscosity is known to approach zero; instead, a slip condition must be used, which relates the eddy stress to the relative velocity.

The Ekman layer in a laminar vortex has been studied by Greenspan & Howard (1963). In the case of small Rossby numbers, i.e. when the overrotation (or underrotation) of the fluid relative to the lower boundary is small compared to the absolute rotation of the boundary itself, they found that the radial volume flux in the Ekman layer over a flat boundary is such that the vertical velocity at the top of the Ekman layer is constant when the fluid above the Ekman layer rotates as a rigid body. As a result, the compensating radial flow above the Ekman layer produces, by advection of angular momentum, an exponential decay with time of the overrotation (or underrotation), with a constant spindown (spinup) time. In a more general vortex, with angular velocity varying with radius, regularity of the velocity field still demands nearly solid rotation in the central part; therefore, the vertical velocity at the top of the Ekman layer is still constant over the central part of the vortex.

The Ekman layer in a turbulent vortex, with a slip condition applied at the bottom surface, was

studied by A. Eliassen (1971). In this case, the vertical velocity at the top of the Ekman layer was found to vanish at the vortex axis and increase linearly with radius; the decay of the overrotation is no longer exponential in time; and the decay rate increases with radius in the central part, being zero at the axis itself. The quoted paper gives quantitative expressions for the strength of the Ekman circulation and the spindown rate.

In the present paper, the Ekman layer, with a slip condition at the bottom surface, is studied by numerical integration of the time-dependent equations. For values of the surface drag coefficient of the order 10^{-3}–10^{-2}, the experiments verify the theoretical results in A. Eliassen (1971). Experiments were also made for a drag coefficient as large as 0.2; in this case the results approach those which can be inferred from the non-slip theory of Greenspan & Howard (1963).

2. DESCRIPTION OF THE FLUID SYSTEM

We consider a homogeneous and incompressible fluid confined between two parallel plane solid boundaries $z=0$ and $z=2H$, of infinite extent. The boundaries will be referred to for convenience as 'horizontal', although gravity plays no role in the problem. Both planes rotate around a 'vertical' axis at a constant absolute angular velocity Ω_s. The motion of the fluid is assumed to be axially symmetric with respect to the axis of rotation. Hence, with r denoting distance from this axis, all fields are functions of r, z, and time t. Moreover, we shall assume that the motion is symmetric with respect to the middle plane $z=H$; hence it suffices to consider the lower half ($0\leq z\leq H$) of the fluid layer.

The absolute fluid velocity in tangential direction will be expressed as $\Omega_s r+u=(\Omega_s+\omega)r$; thus u is the tangential velocity, relative to the boundary, and ω the local relative angular velocity. The absolute angular momentum per unit mass is

$$m=\Omega_s r^2+ur=(\Omega_s+\omega)r^2 \tag{1}$$

The curves $m(r,z,t)=$const. in the rz-plane represent the absolute vortex lines.

The radial velocity v and the vertical velocity w represent a superimposed toroidal circulation. These velocity components must satisfy the condition of incompressibility, and may thus be expressed in terms of a stream function $\psi(r,z,t)$:

$$v=-\frac{1}{r}\psi_z, \quad w=\frac{1}{r}\psi_r \tag{2}$$

where subscripts denote partial derivatives. Note that $\psi=$const. is a streamline in the rz-plane, and that $2\pi(\psi_1-\psi_2)$ represents the volume flux between the streamlines $\psi=\psi_1$ and $\psi=\psi_2$ (or, more precisely, between the two corresponding surfaces of revolution).

Horizontal momentum (tangential and radial) is assumed to be diffused vertically by turbulent eddies, and the eddy viscosity K is assumed constant. On the other hand, horizontal diffusion of horizontal momentum, as well as diffusion of vertical momentum, is ignored. This is in agreement with common practice when dealing with geophysical Ekman layers, the justification being that the vertical scale of such a layer is much smaller than the horizontal scale.

With ϱ denoting the constant density, and p the dynamic pressure, the momentum equations in tangential, radial, and vertical directions become

$$m_t+vm_r+wm_z=Km_{zz} \tag{3}$$

$$v_t+vv_r+wv_z=\frac{m^2}{r^3}-\frac{1}{\varrho}p_r+Kv_{zz} \tag{4}$$

$$w_t+vw_r+ww_z=-\frac{1}{\varrho}p_z \tag{5}$$

The kinematic boundary condition requires that $w=0$ at the bottom boundary, or

$$\psi=0 \quad \text{at} \quad z=0 \tag{6}$$

As a consequence of the symmetry, the net radial volume flux between $z=0$ and $z=H$ must vanish, and hence we also have

$$\psi=0 \quad \text{at} \quad z=H \tag{7}$$

Clearly $\psi=0$ also on the axis, but this need not be imposed as a boundary condition, because it is a consequence of the regularity of the velocity field and will be automatically satisfied.

The remaining boundary conditions concern the flux densities of horizontal momentum.

Suppose that the condition $K=$constant holds

down to a level $z=z_1$, below which there is a shallow Prandtl layer with varying K. At $z=z_1$ we may then apply the familiar expression for the stress in the Prandtl layer

$$K\varrho v_z = C\varrho|\mathbf{v}|v \quad \text{at} \quad z=z_1$$

where C is a drag coefficient for the level z_1. Ignoring the depth of the shallow Prandtl layer, we may apply this condition at $z=0$. Moreover, we shall make use of the approximation $|\mathbf{v}|\approx|u|$ in the expression for the surface stress. For unusually large values of C (>0.02, say), this is not a very good approximation in strong vortices. However, in most cases of geophysical interest, $|v/u|$ is small, and the approximation justified. Thus we obtain the conditions

$$\left.\begin{aligned} m_z &= \frac{Cr^3}{K}|\omega|\omega = \frac{C}{Kr}|m-\Omega_s r^2|(m-\Omega_s r^2) && (8)\\ \psi_{zz} &= \frac{Cr}{K}|\omega|\psi_z = \frac{C}{Kr}|m-\Omega_s r^2|\psi_z && (9)\end{aligned}\right\} \text{ at } z=0$$

Note that the condition for non-slip is obtained by letting $C\to\infty$.

Finally, symmetry at $z=H$ requires that the stresses vanish at this level:

$$\left.\begin{aligned} m_z &= 0 && (10)\\ \psi_{zz} &= 0 && (11)\end{aligned}\right\} \text{ at } z=H$$

The conditions (7), (10), and (11) at $z=H$ will be valid also for a free surface in a gravity field $-g\nabla z$, except that such a surface would not be level but slope downward towards the axis. The effect of this slope would be negligible, however, if the local Froude number ω^2r^2/gH were everywhere small; in this case, our system could alternatively be thought of as a fluid with a free surface at $z=H$.

3. FILTERING OF TOROIDAL INERTIA OSCILLATIONS

We are interested in solutions of the equations of the preceding section which describe the slow evolution of the vortex motion due to the toroidal circulation (v,w) imposed by the Ekman layer. However, the equations are capable of describing also superimposed toroidal inertia oscillations (the vortex is assumed to be rotationally stable, i.e. m_r is everywhere positive). To eliminate these from the outset, we shall use a balanced version of the momentum equations in radial and vertical directions, obtained by ignoring the left-hand sides of eqs. (4) and (5). We shall consider the consequences of this modification.

It follows from the balanced version of eq. (5) that the radial pressure gradient force $-p_r/\varrho$ does not vary with z. It is convenient to express this force in terms of a 'gradient wind angular momentum' $M(r,t)$ such that the corresponding centrifugal force M^2/r^3 would balance the pressure gradient force:

$$\frac{1}{\varrho}p_r = \frac{M^2}{r^3}, \quad M_z=0, \quad (mM>0) \qquad (12)$$

For later reference, we shall also introduce the 'gradient' relative angular velocity $\Omega(r,t)$ which is in equilibrium with the radial pressure force:

$$M=(\Omega_s+\Omega)r^2, \quad \Omega_z=0 \qquad (13)$$

With this notation, and v expressed in terms of ψ from eq. (2), the balanced version of eq. (4) becomes

$$\psi_{zzz} = \frac{m^2-M^2}{Kr^2} \qquad (14)$$

This is an *ordinary* linear differential equation for ψ in the variable z, for any constant values of r and t. If, for a particular r and t, m is known for all z between 0 and H, the *third* order equation (14) together with the *four* boundary conditions (6), (7), (9), and (11) determine ψ for all z, and in addition the constant M.

As a consequence, knowledge of $m(r,z)$ over the entire domain at a certain time enables us to determine $\psi(r,z)$ and $M(r)$ over the domain at the same time. Thus specification of $m(r,z)$ suffices to determine the entire motion field, and also the pressure gradient.

The time evolution of m is governed by (3), which may be written

$$m_t = \frac{1}{r}(m_r\psi_z - m_z\psi_r) + Km_{zz} \qquad (15)$$

4. A HEURISTIC ANALYSIS

We shall assume that m is prescribed initially as a function of r only:

$$m(r,z,0)=m_0(r)=(\Omega_s+\omega_0(r))r^2 \tag{16}$$

To ensure rotational stability, m_0 must be a monotonically increasing function of r.

With this initial condition, eq. (14) and the boundary conditions give

$$M(r,0)=m_0(r), \text{ or, from (13): } \Omega(r,0)=\omega_0(r) \tag{17}$$

and $\psi(r,z,0)=0$ for all r,z, and therefore $v=w=0$ at $t=0$. Thus the eddy stresses vanish initially in the interior, and there is no boundary layer. However, m and ψ will immediately begin to change by the process of eddy diffusion of horizontal vorticity (m_z) from the lower boundary, where the tangential stress is non-zero initially according to (8). The result is the formation of an Ekman boundary layer, where m and v vary with height, and the eddy stress forces in tangential as well as radial direction are significant. Above the Ekman layer is the 'interior' flow where $m(=M)$ and v remain practically independent of height, so that eddy stresses are negligible. The right-hand side of (14) must clearly be non-zero in the Ekman layer; therefore $\psi\neq 0$, and a secondary 'meridional' circulation must exist, which extends also into the interior flow.

On the assumption that m does not depart too much from M in the Ekman layer, (14) may be approximated by the linear equation

$$\psi_{zzz}\approx\frac{2M}{Kr^2}(m-M) \tag{18}$$

applicable in the Ekman layer as well as in the interior.

Moreover, even in the Ekman layer, the vortex lines $m=$constant are typically much steeper than the streamlines $\psi=$constant. On this basis, we may in (15) ignore the vertical advection of angular momentum versus the horizontal (radial) advection; when in addition m_r is approximated by M_r, we obtain the following linear approximation to (15):

$$m_t\approx\frac{1}{r}M_r\psi_z+Km_{zz} \tag{19}$$

In fact, (18) and (19) are precisely the first-order field equations obtained by expanding m, M, and ψ in powers of the drag coefficient C. Therefore, we should expect this approximation to be good for sufficiently small C, but to break down when C is large.

The Ekman layer increases in thickness at first, but after a certain time a quasi-stationary state is reached, where the eddy stress force is closely balanced by advection, so that within the Ekman layer we may write

$$\frac{1}{r}M_r\psi_z+Km_{zz}\approx 0 \tag{20}$$

From (18) and (20) we get a fourth order equation in either ψ_z or $(m-M)$:

$$(m-M)_{zzzz}+\frac{(M^2)_r}{K^2r^3}(m-M)\approx 0 \tag{21}$$

suggesting for the depth of the fully developed Ekman boundary layer a scale:

$$\delta=\left[\text{Real part}\left\{\left(-\frac{(M^2)_r}{K^2r^3}\right)^{1/4}\right\}\right]^{-1}=\sqrt{\frac{2K}{N}} \tag{22}$$

where, from (13)

$$N^2=r^{-3}(M^2)_r=4(\Omega_s+\Omega)^2+2(\Omega_s+\Omega)r\Omega_r \tag{23}$$

is a measure of the rotational stability, expressing the restoring force per unit radial displacement. N plays the same role for rotational stability as the Väisälä-Brunt frequency in the case of gravitational stability. In solid rotation, $N=2(\Omega_s+\Omega)$.

Eq. (22) shows that the Ekman layer depth will decrease with increasing rotational stability. Note also that δ does not depend on H.

We may also estimate a diffusive time scale τ for the formation of a fully developed boundary layer:

$$\tau=\frac{\delta^2}{K}=\frac{2}{N}=\frac{1}{\Omega_s+\Omega}\left(1+\frac{r\Omega_r}{2(\Omega_s+\Omega)}\right)^{-\frac{1}{2}} \tag{24}$$

It is noteworthy that τ depends neither on K nor H.

We shall assume that $H\gg\delta$. In the interior flow above the Ekman layer, we assume $m=M$, $\psi_{zzz}=0$ in agreement with (14). With the boundary conditions (7) and (11), it follows that ψ is a linear function of height in the interior flow, so that v is constant with height, see Fig. 4. Let $h(\sim\delta)$ denote the depth of the fully developed Ekman layer, and let

$\psi(r,h,t)$ be denoted by $\Psi(r,t)$. The latter quantity is a measure of the net radial volume flux in the Ekman layer, or in the interior flow. Then, in the interior flow $h<z<H$,

$$\psi=\frac{H-z}{H-h}\Psi(r,t), \quad v=\frac{\Psi}{(H-h)r} \tag{25}$$

and the angular momentum eq. (15) becomes

$$M_t=-vM_r=-\frac{\Psi M_r}{(H-h)r} \quad \text{when} \quad h<z<H \tag{26}$$

Now Ψ can be estimated by integrating the approximate equation (20) over the Ekman layer $0<z<h$ and using the boundary conditions (6) and (8). This gives

$$\frac{1}{r}M_r\Psi\approx K(m_z)_{z=0}=Cr^3|\omega_{z=0}|\omega_{z=0} \tag{27}$$

We write

$$\omega_{z=0}=\varkappa\Omega \tag{28}$$

where $\varkappa$ is a reduction factor (which tends towards unity when C approaches zero). Thus we obtain the estimate

$$\Psi\approx\frac{\varkappa^2C|\Omega|\Omega r^4}{M_r}=\frac{\varkappa^2C|\Omega|\Omega}{2(\Omega_s+\Omega)+r\Omega_r}r^3 \tag{29}$$

We note that according to this expression, Ψ depends neither on K nor H, but only on C and the distribution of Ω in the vortex. With $M_r>0$, Ψ and Ω are of the same sign. Hence, if the fluid rotates faster than the bottom surface (over-rotation, $\Omega>0$), Ψ is positive and the secondary flow is directed mainly towards the axis in the Ekman layer and away from it in the interior. By under-rotation ($-\Omega_s<\Omega<0$), the meridional circulation is in the opposite sense.

When (29) is entered into (26), and M_t is expressed as $\Omega_t r^2$, we find

$$\Omega_t\approx-\frac{\varkappa^2Cr}{H-h}|\Omega|\Omega \tag{30}$$

or, integrated from an initial value Ω_0:

$$\frac{1}{|\Omega|}\approx\frac{1}{|\Omega_0|}+\frac{\varkappa^2Crt}{H-h}, \quad (\text{with } \Omega\Omega_0>0) \tag{31}$$

Here Ω_0 may be of either sign. According to this approximate formula, $|\Omega|$ will in any case decay with time, so that there is a spinup in the case of underrotation and spindown in the case of over-rotation relative to the boundary. The time required to reduce $|\Omega|$ by a factor of two is

$$t_{\frac{1}{2}}=\frac{H-h}{\varkappa^2Cr|\Omega|}\approx\frac{H}{Cr|\Omega|} \tag{32}$$

As would be expected, $t_{\frac{1}{2}}$ is proportional to the depth $(H-h)$ of the interior fluid. It is less obvious that $t_{\frac{1}{2}}$ is inversely proportional to the relative velocity $r|\Omega|$; therefore, $t_{\frac{1}{2}}$ increases towards the axis, and on the axis itself, there is no spinup/spindown at all. Moreover, it is noteworthy that K does not appear in (31) and (32).

Eq. (31) was derived by A. Eliassen (1971) by a similar heuristic argument. In the same paper, the steady-state problem ($H=\infty$) was solved by expansion of ω, v, and w in powers of r. The solution is valid also for large Rossby numbers. The value $W(r,t)$ of w at the top of the Ekman layer was found to be

$$W=\tfrac{3}{2}C\frac{|\Omega_{r=0}|\Omega_{r=0}}{\Omega_s+\Omega_{r=0}}r+O(r^2) \tag{33}$$

This formula is in agreement with (29), i.e. $W=r^{-1}\Psi_r$, when $\varkappa=1$.

A similar heuristic analysis can be made if the boundary condition (8) is replaced by a non-slip condition at the bottom. However, in this case the Rossby number ($|\Omega|/\Omega_s$) would have to be assumed small, in order that replacement of m_r by M_r in the Ekman layer (eq. (20)) should be a valid approximation. For small Rossby numbers, $N=2\Omega_s$, and $\delta=(K/\Omega_s)^{\frac{1}{2}}$. In (27), we might then set: $(m_z)_{z=0}=(M-\Omega_s r^2)/\delta$. Instead of (29) we would then have

$$\Psi\approx\frac{Kr(M-\Omega_s r^2)}{M_r\delta}=(K\Omega_s)^{\frac{1}{2}}\frac{\Omega r^3}{M_r} \tag{34}$$

and hence, from (26),

$$\Omega_t=-\frac{\sqrt{K\Omega_s}}{H-h}\Omega \tag{35}$$

expressing exponential decay, independent of r, in agreement with the rigorous theory of Greenspan and Howard. Comparison with (29) and (30) shows the remarkable difference between the 'laminar' and the 'turbulent' case.

5. NONDIMENSIONAL VARIABLES

Eqs. (14) and (15) with the boundary conditions (6–11) contain the three constants Ω_s, K, and C. It is convenient to take as units of time and length

$$T=\Omega_s^{-1}, \quad L=K^{\frac{1}{2}}\Omega_s^{-\frac{1}{2}} \tag{36}$$

For instance, if we take $\Omega_s=1.9\times10^{-5}$ s^{-1}, $K=20$ m^2 s^{-1}, which might be representative values for a hurricane, we get $L=1$ km, $T=15$ hours, and the velocity unit $LT^{-1}=0.02$ ms^{-1}.

Henceforth, all variables will be expressed as nondimensional numbers in these units. As a consequence, Ω_s and K will not appear explicitly in the equations, their values in these units being unity. Thus only the single parameter C remains. However, the initial condition (58) introduces another time and space scale.

6. NUMERICAL SOLUTION OF THE FILTERED INITIAL VALUE PROBLEM

The filtered initial value problem was solved numerically for a number of cases, using finite difference analogues of eqs. (14), (15), and the boundary conditions (6–11). The calculations were made for a rectangular grid of points in the rz-plane. Since gradients are small in the outer part of the vortex, it is desirable to let the mesh-size increase with r. Therefore the gridpoints were spaced uniformly in $\ln r$. In the vertical, the points were spaced uniformly in z, however, with a changeover from a small mesh-size in the Ekman layer to a larger mesh-size above it.

Specifically, the ψ-values were specified in gridpoints (r_i, z_j) where

$$r_i=r_0e^{\mathrm{li}}, \quad i=0,1,\ldots,I \tag{37}$$

$$z_j=\begin{cases}\Delta z_1 j, & j=0,1,\ldots,N\\ \Delta z_1 N+\Delta z_2(j-N), & j=(N+1),\ldots,J\end{cases} \tag{38}$$

The m-values, on the other hand, were specified in the points $(r_i, z_{j+\frac{1}{2}})$, $j=0,1,\ldots,(J-1)$.

Numerical solution of the balance equation

For an arbitrary r_i, the balance equation (14) is replaced by the finite difference analogue

$$(\Delta^3\psi)_{j+\frac{1}{2}}=\frac{(\Delta z)^3}{r^2}(m^2_{j+\frac{1}{2}}-M^2), \quad j=0,1,\ldots,(J-1) \tag{39}$$

where, in the case of uniformly spaced gridpoints,

$$(\Delta^3\psi)_{j+\frac{1}{2}}=\psi_{j+2}-3\psi_{j+1}+3\psi_j-\psi_{j-1} \tag{40}$$

This expression for $\Delta^3\psi$ must be modified in the points $N\pm\frac{1}{2}$, due to the change of vertical mesh-size at $j=N$; in any case, $\Delta^3\psi$ is written so as to yield the exact value for a cubic polynomial.

Application of (39) at the levels $j=0$ and $j=J-1$ implies the use of auxiliary ψ-values (ψ_{-1} and ψ_{J+1}) outside the boundaries. These are obtained from the boundary conditions, as shown below.

To calculate the ψ-values and M when all $m_{j+\frac{1}{2}}(j=0,1,\ldots,(J-1))$ are given, we write

$$\psi_j=\varphi_j+\chi_j \tag{41}$$

where φ_j satisfies

$$(\Delta^3\varphi)_{j+\frac{1}{2}}=\frac{(\Delta z)^3}{r^2}(m^2_{j+\frac{1}{2}}-m^2_{j-\frac{1}{2}}) \tag{42}$$

with

$$\varphi_{J-1}=\varphi_J=\varphi_{J+1}=0 \tag{43}$$

The values of $\varphi_{J-2}(=0), \varphi_{J-3}, \ldots, \varphi_0, \varphi_{-1}$ are readily obtained from (42), starting from the top and working down.

The function χ_j satisfies

$$(\Delta^3\chi)_{j+\frac{1}{2}}=\frac{(\Delta z)^3}{r^2}(m^2_{J-\frac{1}{2}}-M^2)=\text{constant}. \tag{44}$$

Hence, χ_j is a cubic polynomial. To satisfy the conditions (6), (7), and (11), i.e.

$$\varphi_0+\chi_0=0, \quad \chi_J=0, \quad \chi_{J-1}+\chi_{J+1}=0 \tag{45}$$

we write χ_j in the form

$$\chi_j=\left(1-\frac{z_j}{H}\right)\left[b\frac{z_j}{H}\left(2-\frac{z_j}{H}\right)-\varphi_0\right] \tag{46}$$

where the constant b is determined from the following finite difference form of (9) (with $\psi_0=0$):

$$\psi_1+\psi_{-1}=\gamma\psi_1, \quad \gamma=\frac{C\Delta z_1}{r}|m_{\frac{1}{2}}-r^2| \tag{47}$$

The result is

$$b=\frac{\varphi_1+\varphi_{-1}-2\varphi_0-\gamma\left[\varphi_1-\varphi_0\left(1-\frac{\Delta z_1}{H}\right)\right]}{6\left(\frac{\Delta z_1}{H}\right)^2+\gamma\frac{\Delta z_1}{H}\left(1-\frac{\Delta z_1}{H}\right)\left(2-\frac{\Delta z_1}{H}\right)} \tag{48}$$

Thus all φ_j and χ_j can be found, and ψ_j is obtained from (41).

Finally, it follows from (44) and (45) that

$$M^2 = m_{j-\frac{1}{2}}^2 - \frac{6r^2}{H^3} b \tag{49}$$

Integration of the prognostic momentum equation

The momentum equation (15) was integrated in steps of time,

$$t_k = k\Delta t \tag{50}$$

using forward time differencing:

$$m_{i,j+\frac{1}{2}}^{k+1} = m_{i,j+\frac{1}{2}}^{k} + \left(\frac{\partial m}{\partial t}\right)_{i,j+\frac{1}{2}}^{k} \Delta t \tag{51}$$

Eq. (15) was written as

$$\left(\frac{\partial m}{\partial t}\right)_{i,j+\frac{1}{2}} = \frac{1}{r_i^2 l \Delta z}[(\psi_{i,j+1} - \psi_{i,j})\Delta_r m$$
$$-\tfrac{1}{4}(\psi_{i+1,j+1} + \psi_{i+1,j} - \psi_{i-1,j+1} - \psi_{i-1,j})\Delta_z m]$$
$$+ \frac{1}{(\Delta z)^2}[m_{i,j+\frac{3}{2}} - 2m_{i,j+\frac{1}{2}} + m_{i,j-\frac{1}{2}}] \tag{52}$$

where $\Delta_r m$ and $\Delta_z m$ are non-centered, upstream differences in the directions r and z, respectively.

Due to the change of vertical mesh-size at $j=N$, the expression for $\partial^2 m/\partial z^2$ in (52) had to be modified in points $j+\frac{1}{2}=N\pm\frac{1}{2}$.

Application of (52) in the lowest gridpoints $(i,\frac{1}{2})$ requires knowledge of $m_{i,-\frac{1}{2}}$. These values are obtained from the boundary condition (8) in the finite difference form:

$$m_{i,-\frac{1}{2}} = m_{i,\frac{1}{2}} - \frac{C\Delta z_1}{r_i}|m_{i,\frac{1}{2}} - r_i^2|(m_{i,\frac{1}{2}} - r_i^2) \tag{53}$$

Likewise, when applying (52) in points $(i, J-\frac{1}{2})$, we need to know $m_{i,J+\frac{1}{2}}$, which is obtained from (10) in the form

$$m_{i,J+\frac{1}{2}} = m_{i,J-\frac{1}{2}} \tag{54}$$

The vertical boundaries. With the gridpoints uniformly spaced in the coordinate $\ln r$, the axis itself cannot be included; the innermost gridpoints $r=r_0$ form a vertical boundary on the inside. This was treated as an open boundary. In points of inflow, $v>0$, the upstream difference $\Delta_r m$ on this boundary was calculated on the assumption that $\partial/\partial r(m/r^2)=0$, i.e.

$$\Delta_r m = m_{0,j+\frac{1}{2}} - m_{-1,j+\frac{1}{2}} = m_{0,j+\frac{1}{2}}(1-e^{-2l}) \tag{55}$$

The outer boundary of the grid $r=r_I$ was also treated as an open boundary. In points of inflow ($v<0$), $\partial m/\partial r$ was assumed to vanish, so that

$$\Delta_r m = 0 \tag{56}$$

On both vertical boundaries, w in the advective term of (52) was calculated from a non-centered difference in ψ.

The start. With an initial condition $m_{ij}^0 = m_0(r_i)$, we obtain $\psi_{i,j}^0 = 0$ for all i,j. However, from (53), $m_{i,-\frac{1}{2}}^0 \neq m_0$. Therefore, the finite difference approximation to $\partial^2 m/\partial z^2$ in (52) is not zero in the point $j=\frac{1}{2}$. It follows that $(\partial m/\partial t)_{i,\frac{1}{2}}^0 \neq 0$, so that already after the first time step, m varies with height, and $\psi_{i,j}^1 \neq 0$.

Numerical values. The non-dimensional grid constants were chosen as follows

$$l = 0.076\,, \quad I = 71$$
$$r_0 = 2.5\,, \quad r_I = r_0 e^{\mathrm{II}} = 539.3$$
$$\Delta z_1 = 0.1\,, \quad \Delta z_2 = 0.5$$
$$N = 14\,, \quad J = 21\,, \quad H = 4.9$$

The gridpoints are shown in the axes of Fig. 7. The time step is restricted not only by the Courant–Friedrichs–Lewy criterion, but also by the following requirement

$$\Delta t < \frac{2\pi^2}{H^2 N_{\max}^2} \tag{57}$$

where $N_{\max}$ is the highest value of the inertia frequency N (eq. 23). A demonstration of (57) is given in the Appendix. Since the condition requires $\Delta t \sim H^{-2}$, the amount of computation increases rapidly with increasing H. It was for this reason that we had to take for H a value as small as 4.9, although a larger value would have been preferred.

7. THE INITIAL STATE

The initial condition was taken to be

$$m_0(r) = (1+\omega_0(r))r^2\,, \quad \omega_0(r) = \frac{Ro}{1+\left(\frac{r}{a}\right)^2} \tag{58}$$

where Ro and a are positive constants. The Rossby number Ro measures the relative angular velocity at the center, in units of Ω_s. The relative tangential velocity $r\omega_0$ has its maximum value $\frac{1}{2}Roa$ at the distance $r=a$. Integrations were performed with the four Ro-values: $Ro=1$, 5, 10, and 20. In all runs, a was taken to be 50.

The initial vortex is rotationally stable; from (23),

$$N^2=4\left(1+\frac{Ro}{1+\left(\frac{r}{a}\right)^2}\right)\left(1+\frac{Ro}{\left(1+\left(\frac{r}{a}\right)^2\right)^2}\right)>4 \tag{59}$$

Since $N>2$ for all r, it follows from (22) and (24) that $\delta<1$, $\tau<1$.

Fig. 1 shows the boundary layer depth scale δ as a function of r from eq. (22) for the four values of Ro. From these curves, we must expect the Ekman layer depth to increase from the center and out, and also to increase with decreasing Ro.

Fig. 2 shows τ, the time scale for formation of the Ekman layer as a function of r and Ro, according to (24). The smallest values are found in the center, where $\tau=(1+Ro)^{-1}$; there τ is the time required for the fluid to rotate one radian in the absolute sense.

Integrations were made for four different values of C, viz: 0.002, 0.006, 0.02, and 0.2. According to (32), the time required for reducing ω_0 to half its original value is of the order

$$t_{\frac{1}{2}}\approx\frac{H}{C r\omega_0}=\frac{H\left(1+\left(\frac{r}{a}\right)^2\right)}{C\,Ro\,r} \tag{60}$$

Fig. 3 shows the ratio $\tau/t_{\frac{1}{2}}$ as a function of r for $a=50$, $C=0.002$, and $Ro=1$, 5, 10, and 20. All val-

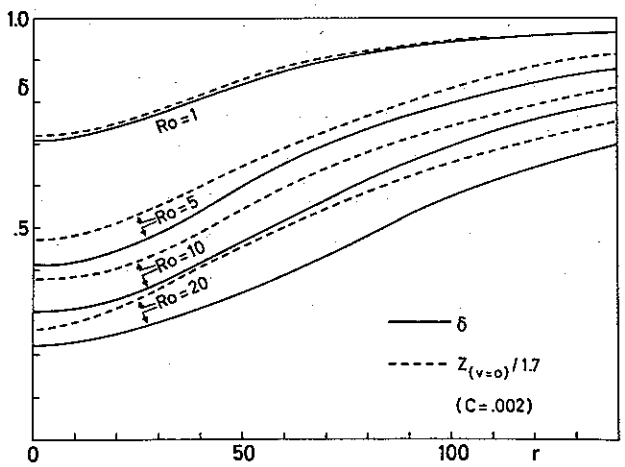

Fig. 1. Solid curves: The non-dimensional boundary layer depth scale δ as a function of r and Ro according to eq. (22). Dotted curves: The level at which $v=0$ (divided by 1.7 for easier comparison), as a function of r and Ro, from numerical integrations with $C=0.002$.

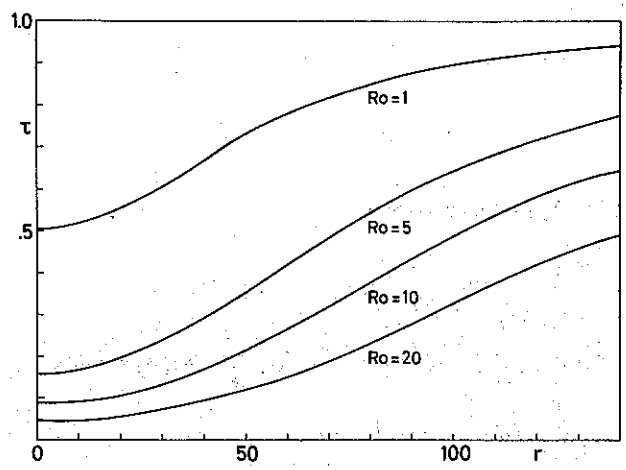

Fig. 2. The non-dimensional time scale for formation of the Ekman layer, τ, as a function of r and Ro, according to eq. (24).

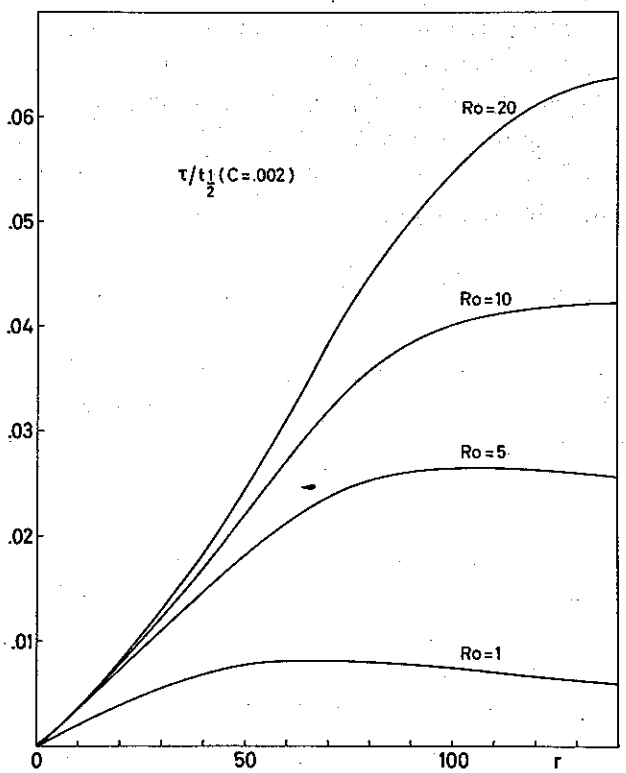

Fig. 3. The ratio $(\tau/t_{\frac{1}{2}})$ of the two time scales defined by (24) and (32), as a function of r and Ro for $C=0.002$.

ues are small, indicating a good separation between the adaptation time scale τ of the Ekman layer and the spindown time scale $t_{\frac{1}{4}}$. Therefore, we expect the Ekman layer to be only slightly affected by the spindown process; the fully developed Ekman layer is adjusted to the interior flow as if it were stationary, and the Ekman layer structure is insensitive to changes in H.

For $C=0.02$, the values of Fig. 3 should be multiplied by 10, showing that the separation of the time scales is no longer as good for large Ro. Finally, for $C=0.2$, the values of Fig. 3 must be increased by a factor of 100, so that the two time scales are of the same order. In this case, we must expect that the boundary layer structure will depend much upon the arbitrary choice $H=4.9$.

Table 1. Time step (Δt) and integration time (T) for the fourteen combinations of drag coefficient (C) and Rossby number (R_0) for which computations were made

C	Ro =	1	5	10	20
0.002	Δt	0.004	0.004	0.001	0.0005
	T	4.8	4.8	0.8	0.4
0.006	Δt			0.001	0.0005
	T			0.8	0.4
0.02	Δt	0.004	0.004	0.002	0.0005
	T	3.2	1.4	0.9	0.4
0.2	Δt	0.004	0.002	0.002	0.0005
	T	2.0	1.0	0.8	0.4

8. RESULTS

Integrations were made for the 14 combinations of C and Ro shown in Table 1, which also gives the time step and the integration time T for each case. In all cases the nondimensional a was set equal to 50.

In all 14 runs, the toroidal Ekman circulation grew to a maximum strength within a time of the order τ, and then slowly decayed without much change of shape as a result of the spindown process.

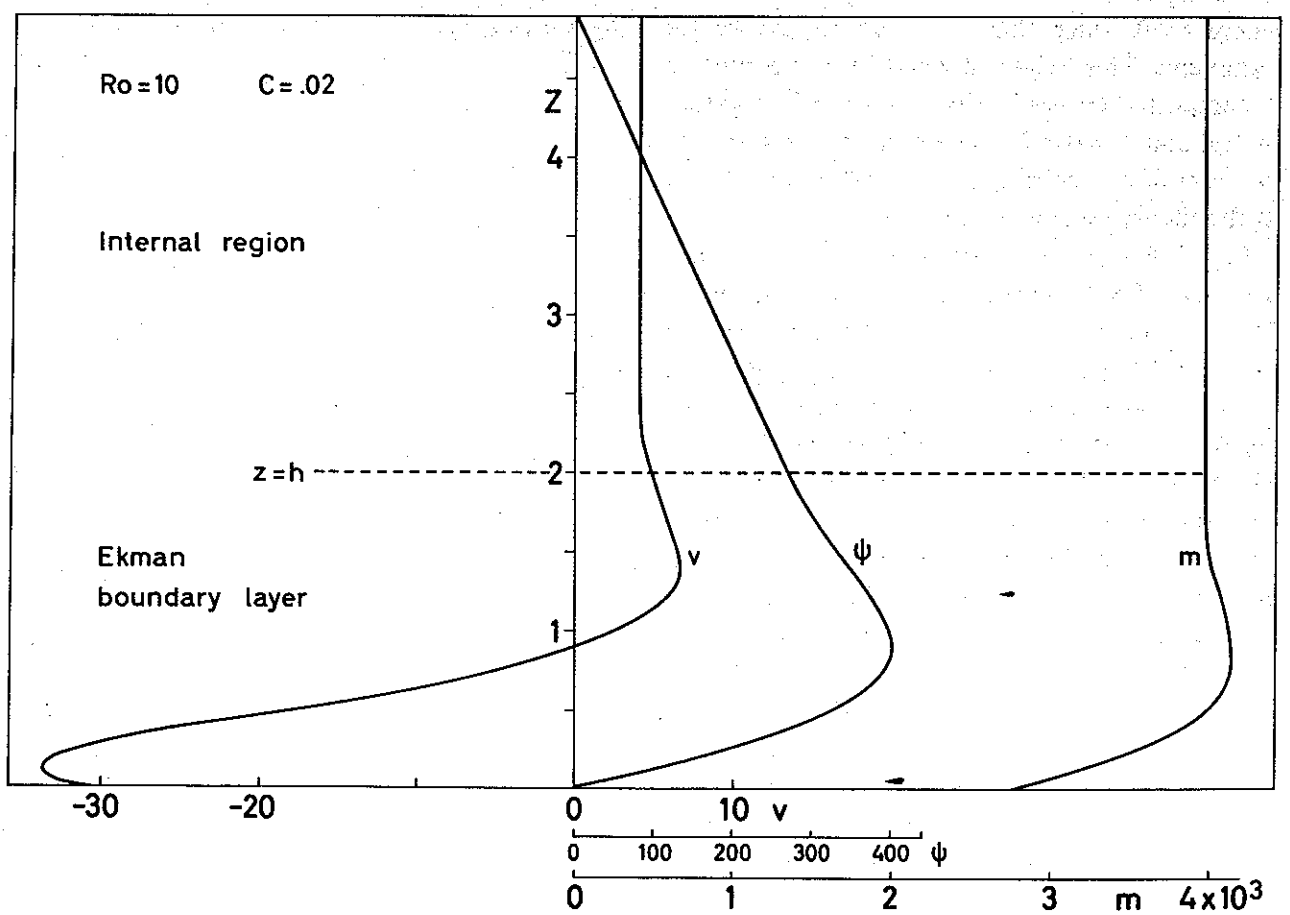

Fig. 4. Non-dimensional v, ψ, and m as function of z for $Ro=10$, $C=0.02$, $r=22.5$, $t=0.9$.

After the formative stage, it was a common feature of all computed fields that v and m varied with height in the lower part, but were constant in the upper part, thus showing a clear-cut subdivision into a lower Ekman boundary layer and an upper interior regime. An example is shown in Fig. 4 where v, ψ, and m are plotted against height for the case $Ro=10$, $C=0.02$, $r=22.5$, $t=0.9$. The curves suggest an Ekman layer depth $h=2.0$.

Fig. 5 shows computed Ekman spiral hodographs $(u-U, v)$ for five different radial distances for $C=0.002$ and $Ro=1$; and Fig. 6 shows the same for $Ro=10$. In spite of the great difference in Ro, the spirals are quite similar.

An example of the computed fields of m, ψ, v, and w is shown in Figs. 7–9, for the case $Ro=10$, $C=0.002$, $t=0.3$.

It is apparent from these figures that the Ekman layer depth increases with r; and this was a common feature of the computed fields in all cases. This is in qualitative agreement with the theoretical values of δ shown in Fig. 1. To obtain a quantitative comparison, δ was compared with the height where $v=0$, since this is a well-defined height parameter. This height (divided by 1.7) is plotted as the dotted curves in Fig. 1, for the four values of Ro, and $C=0.002$; the similarity between the two sets of curves is apparent, and gives support to the theoretical expression (22).

Figs. 7–9 refer to a time when the Ekman circulation had almost reached its maximum strength. The maximum value of the stream function ($\psi_{\max}=1710$) is a measure of the total volume flux in the Ekman circulation. As the circulation builds up, $\psi_{\max}$ increases to an overall maximum which will be denoted by ψ_M; the coordinates of the maximum point are denoted by r_M, z_M, t_M. Likewise, we may at each time instant identify a point of maximum rising motion. Its value reaches a peak w_M (in a point r_w, z_w) roughly at the time t_M of maximum volume flux.

Table 2 summarizes the values of $t_M, \psi_M, r_M, z_M, w_M, r_w, z_w$ for all 14 runs.

Fig. 10 shows ψ_M as a function of Ro and C. For small values of C, ψ_M increases with Ro almost as Ro^2; this is clearly due to the non-linear boundary condition (8). For larger values of C, the increase of ψ_M with Ro is almost linear, and one might expect that the curves for large C would approach the straight line (dashed).

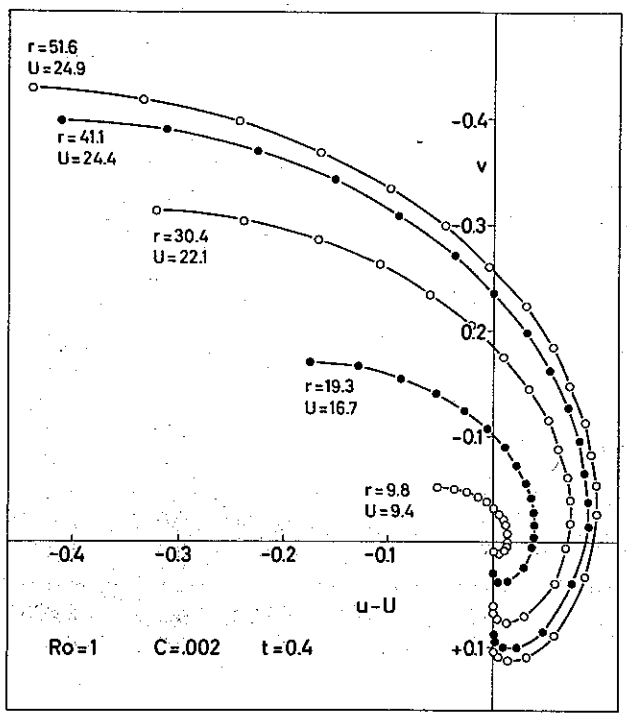

Fig. 5. Ekman spirals for $Ro=1$, $C=0.002$, $t=0.4$.

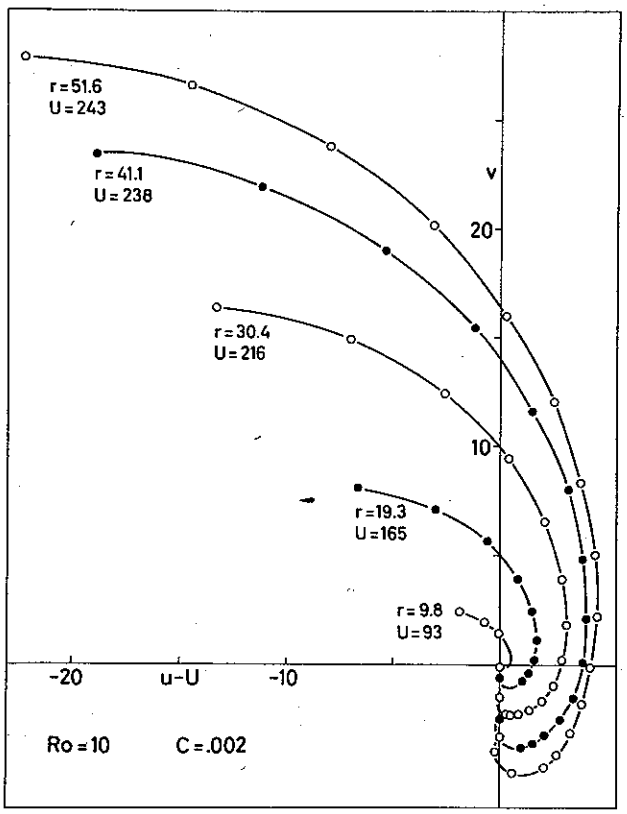

Fig. 6. Ekman spirals for $Ro=10$, $C=0.002$, $t=0.3$.

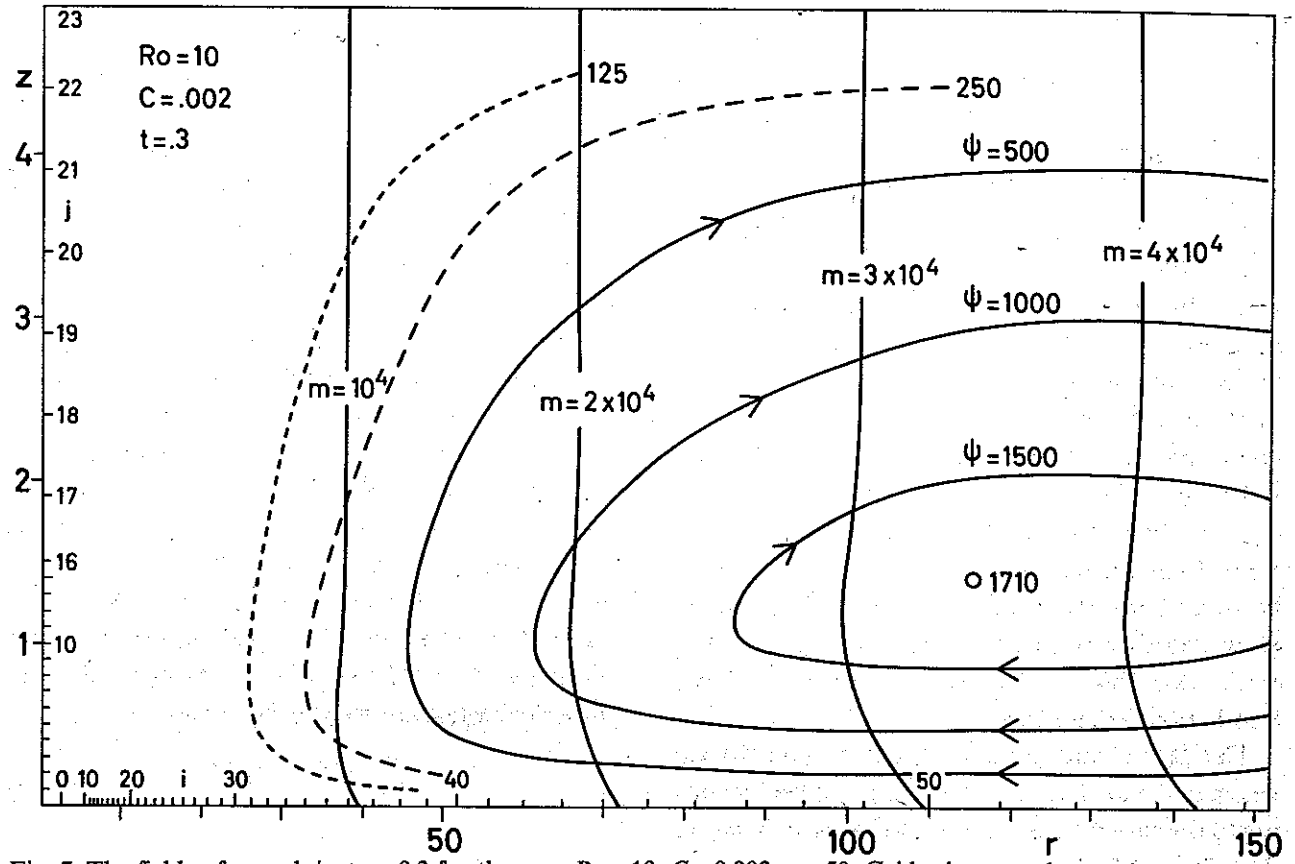

Fig. 7. The fields of m and ψ at $t=0.3$ for the case $Ro=10$, $C=0.002$, $a=50$. Gridpoints are shown along the axes.

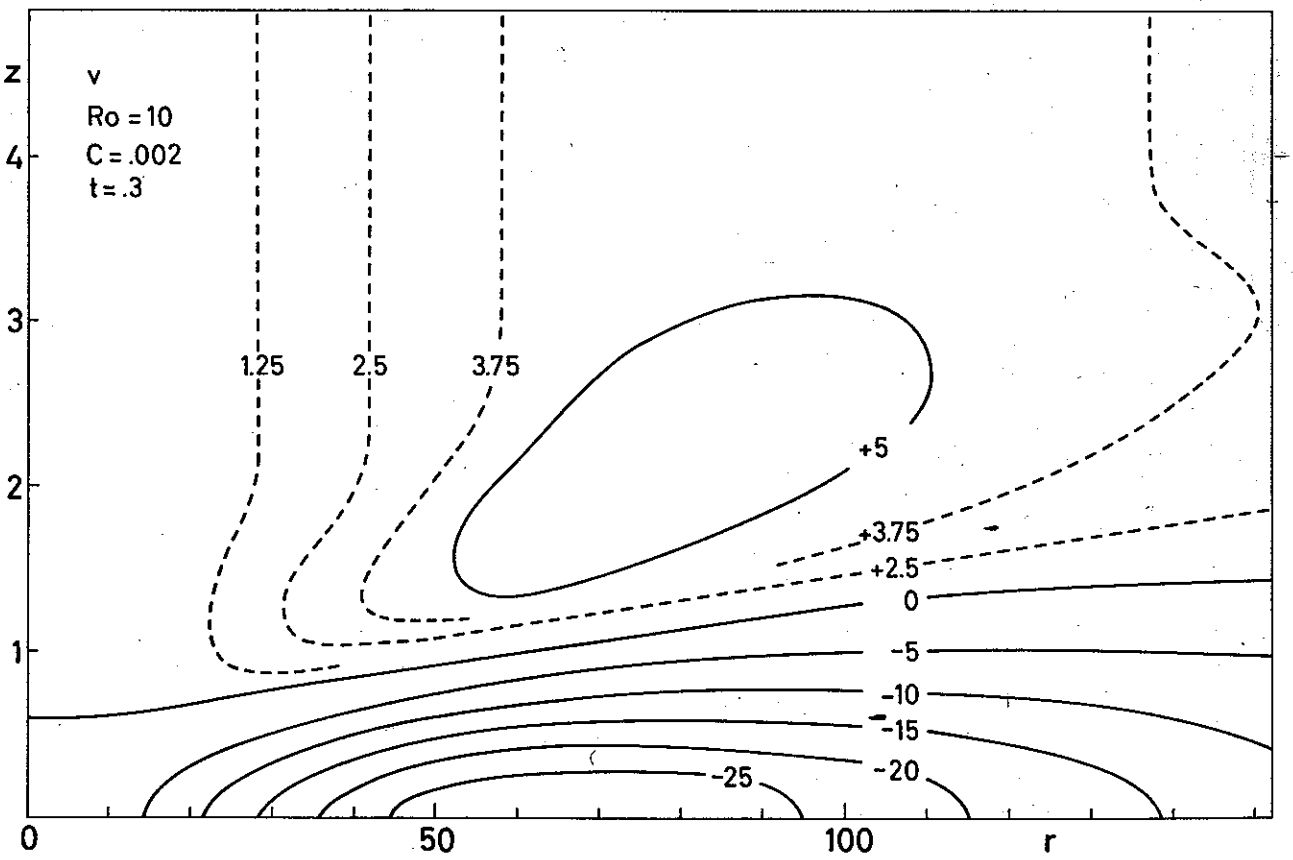

Fig. 8. The field of v at $t=0.3$. Same case as Fig. 7.

One of the main objectives of the study was to investigate the distribution of vertical velocity in the central part of the vortex. In Fig. 11a, b, c, d, the solid curves show, for the various combinations of c and Ro, the computed vertical velocity as a function of radius at the level z_w where w has its maximum, and at a time when the Ekman circulation was fully developed. Although the calculations were not extended to the center, but only to $r=2.5$, the curves confirm the theoretical result that $w \sim r$ in the central part of the vortex. The curves also show that the central part of the vortex, where $w \sim r$, decreases in size as C increases. In the limit $C \to \infty$, we may thus assume that the radius of the central part, where $w \sim r$, tends to zero, so that w becomes constant in agreement with Greenspan–Howard's theory based on the non-slip boundary condition. This resolves the apparent contradiction between these theories.

The dashed straight lines of Fig. 11 give the values of $\partial w/\partial r$ at the top of the Ekman layer, according to the theoretical expression (33), which in non-dimensional form is

$$W_{\text{theory}} = \tfrac{3}{2} C \frac{Ro^2}{1+Ro} \cdot r \tag{61}$$

Although the agreement is not perfect, it is apparent that (61) gives a very good estimate of $\partial w/\partial r$ in all cases considered; in particular, it should be stressed that the agreement is good even for large Rossby numbers, as demanded by the theory.

Next we shall consider the spindown process and the accuracy of the theoretical formula (31). Two examples are shown in Fig. 12. The curves show Ω as a function of radius at $t=0$ and at a later time t for two cases: $Ro=20$, $C=0.002$, $t=0.4$, and $Ro=10$, $C=0.002$, $t=0.8$. In both cases, the decay of Ω with time is fastest at the axial distance where Ωr is largest, and there is no decay at the center.

In order to test the theoretical eq. (31), we have calculated, from the Ω-values obtained from the numerical integrations, the expression

$$H' = \frac{Cr(t_2 - t_1)}{\dfrac{1}{\Omega_2} - \dfrac{1}{\Omega_1}} \tag{62}$$

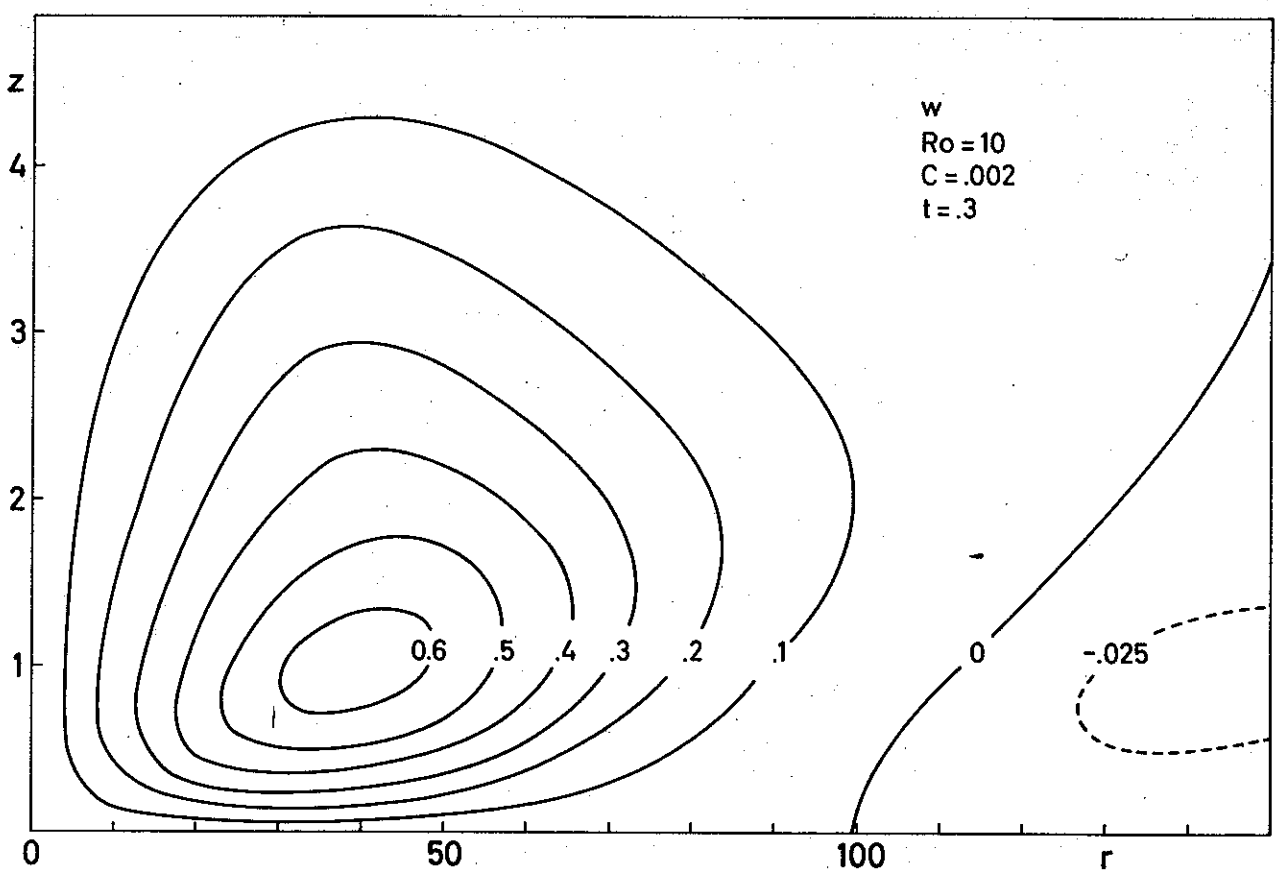

Fig. 9. The field of w at $t=0.3$. Same case as Fig. 7.

Table 2. Summary of results from numerical integrations.

C	Ro	t_M	ψ_M	r_M	z_M	w_M	r_w	z_w
0.002	1	1.0	25	95	1.4	0.017	26	1.3
	5	0.6	512	110	1.4	0.23	35	1.1
	10	0.45	1730	120	1.35	0.63	41	1.0
	20	0.35	5490	140	1.3	1.6	44	0.8
0.006	10	0.4	3470	130	1.4	1.4	33	0.9
	20	0.35	9610	150	1.4	3.2	35	0.8
0.02	1	0.6	175	100	1.4	0.13	22	1.3
	5	0.4	2100	120	1.4	1.1	24	1.1
	10	0.4	5390	140	1.4	2.4	26	0.9
	20	0.35	13100	160	1.4	4.3	26	0.8
0.2	1	0.6	488	150	1.9	0.36	13	1.3
	5	0.5	3230	190	1.9	1.8	13	1.1
	10	0.5	6980	190	1.9	3.0	15	1.0
	20	0.4	15100	190	1.9	5.2	19	0.9

Here Ω_1 and Ω_2 are the values of Ω (or ω at $z=H$) at the times t_1 and t_2, respectively. The result is shown in Table 3, for five values of r and twelve combinations of Ro and C. Note that if (31) were correct, we should have $H'=(H-h)/\varkappa^2$. The table shows that the values of H' are remarkably constant for $C=0.002$, indicating that (31) is indeed a good approximation. With $H=4.9$, $h\approx 1$, the value $H'=5.2$ is consistent with a value 0.87 for the reduction factor $\varkappa$, a rather reasonable figure.

For $C=0.02$, H' is still quite uniform in the central part of the vortex, whereas for $C=0.2$ the values vary so much that eq. (31) is clearly not applicable. This is not surprising, because (31) is derived as an approximation for small C.

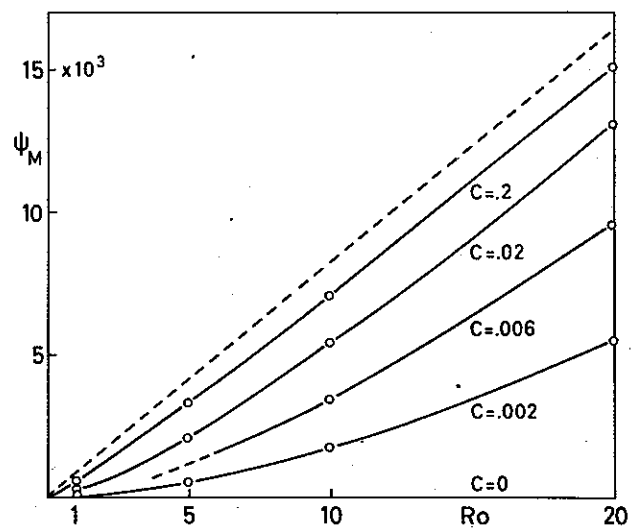

Fig. 10. Maximum volume transport ψ_M as a function of Ro and C. Dashed line: extrapolated for $C\to\infty$.

9. FINAL REMARKS

The numerical computations have given strong support to the approximate theoretical expression based on (18) and (19), which may be obtained from the filtered equations by expansion in terms of the drag coefficient C. In particular, the computations performed with small values of C verify eq. (22) for the Ekman layer depth scale, eq. (31) for the spindown rate, and eq. (33) for the vertical motion near the axis. This may be considered as a verification also of eq. (29) for the total mass flux in the Ekman layer.

Note that since the spindown rate increases with r, the rotational stability of the vortex will decrease with time. As M_r decreases, eq. (29) predicts that the Ekman circulation will grow in strength. However, when M_r tends towards zero, the approximation leading to (29) and (31) breaks down.

It was hoped at the outset that a clue could be found as to what determines the radius where the ascending motion is strongest. This would be the value of r for which

$$\frac{\partial}{\partial r}\left(\frac{1}{r}\Psi_r\right)=0$$

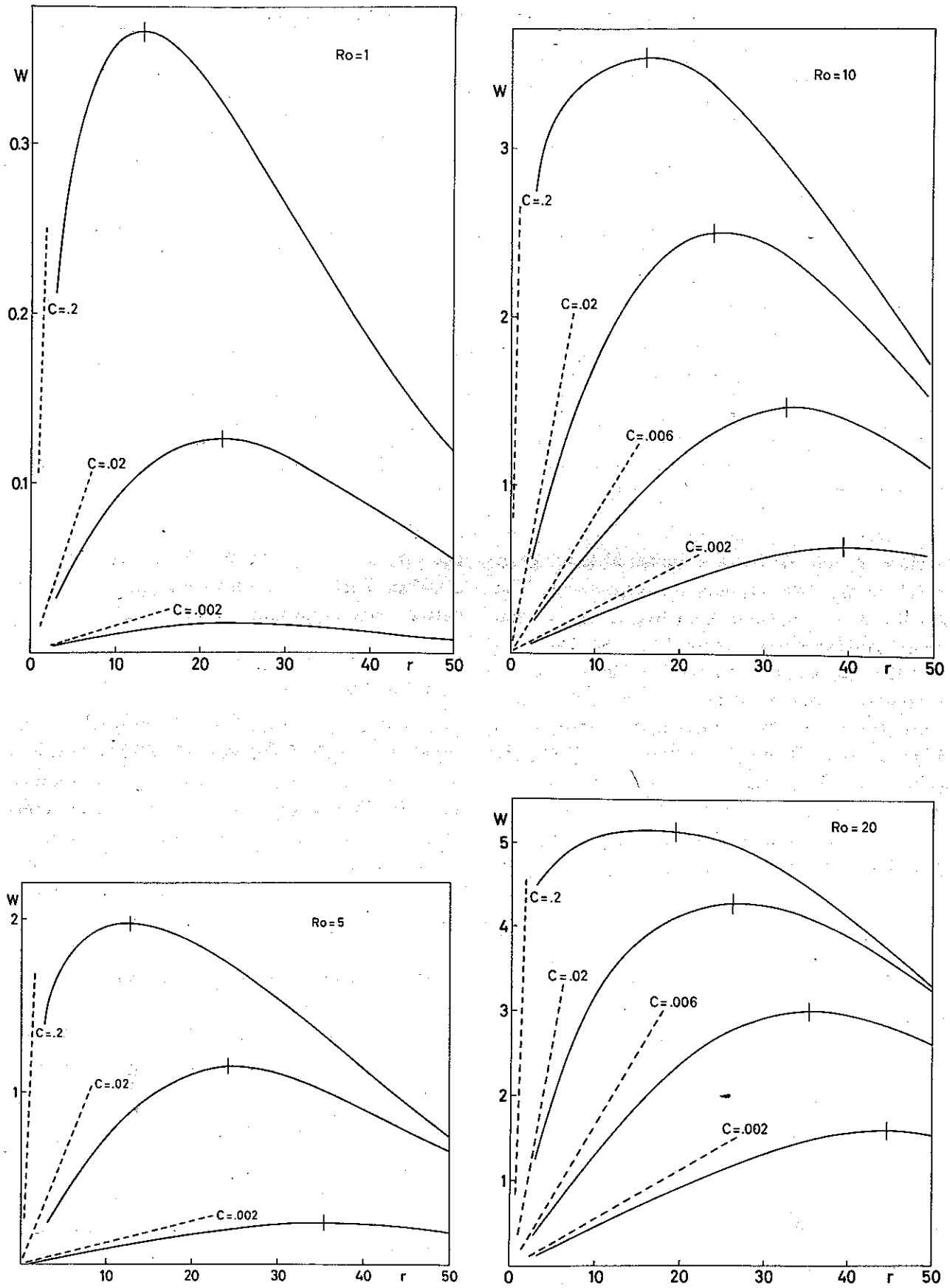

Fig. 11. Solid curves: computed values of w at the level of w_{max}, as a function of r. a: $Ro=1$, b: $Ro=5$. c: $Ro=10$. d: $Ro=20$. Dashed lines: $W(r)$ according to (61).

Table 3. H′ from eq. (62)

C	Ro	t_1	r=	2.7	10.5	47.9	102.0	217.5
			t_2					
0.002	1	1.0	4.0	5.3	5.3	5.3	5.4	5.3
	5	0.4	4.8	5.2	5.2	5.4	5.7	5.5
	10	0.3	0.8	5.2	5.2	5.2	6.2	5.8
	20	0.2	0.4	5	5	5	6	–
0.02	1	0.8	3.2	5.4	5.7	6.8	6.6	6.0
	5	0.1	1.4	5.4	6.1	9.4	12	9.5
	10	0.3	0.9	5.3	6.1	10	16	13
	20	0.15	0.4	5.2	5.9	12	23	20
0.2	1	0.6	2.0	6.5	10	20	20	14
	5	0.3	1.0	7.7	17	51	60	45
	10	0.3	0.8	8.0	19	65	111	86
	20	0.125	0.4	8.4	23	86	186	180

According to (29), this value of r will depend upon $\Omega(r)$, which again by (31) depends on the length scale a introduced by the initial condition.

APPENDIX

Derivation of the stability condition (57)

In the first integrations computational instability was encountered, although the CFL-condition as well as the stability condition for the diffusion equation were both satisfied. The unstable mode had the form $\sin \pi z/H$ in ψ, or $\cos \pi z/H$ in v; thus it manifested itself as the *largest* possible wave length $2H$, a somewhat unusual phenomenon. Also, the instability showed up first near the inner boundary $r=2.5$.

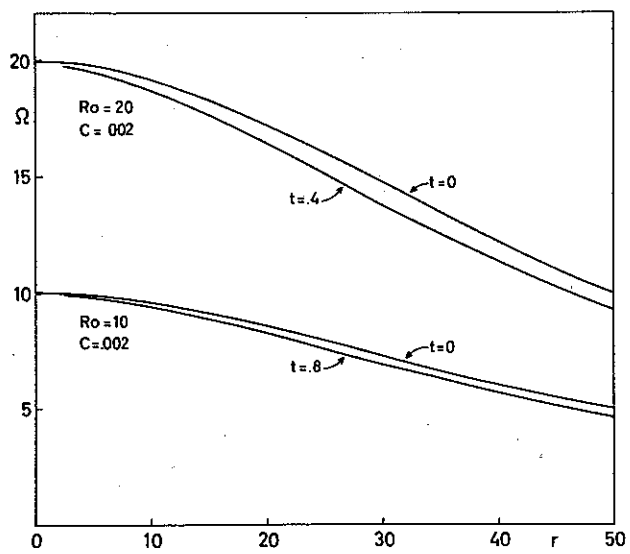

Fig. 12. The decay of $\Omega(r)$ with time in two cases.

It turns out that this instability is a linear phenomenon which can be explained from the linearized version (18) and (19) of the equations. We consider a superimposed disturbance m', ψ' and $v'=-1/r\psi'_z$, which is harmonic in z such that $\partial^2/\partial z^2=-\alpha^2$. There can be no such disturbance in M, which is by definition constant in z. Therefore, the linearized equations (18), (19) for the disturbance become, in dimensional notation

$$v'_{zz}=-\alpha^2 v'=\frac{2M}{Kr^3}m' \tag{A1}$$

$$m'_t=-M_r v'-K\alpha^2 m' \tag{A2}$$

whence, by eliminating v'

$$m'_t=-\frac{m'}{T}$$

where, from (23)

$$\frac{1}{T}=\frac{2MM_r}{Kr^3\alpha^2}+K\alpha^2=\frac{N^2}{K\alpha^2}+K\alpha^2 \tag{A3}$$

Thus the disturbance decays as $\exp(-t/T)$. A numerical integration in forward time steps Δt will clearly be unstable unless $\Delta t<2T$. Since the vertical wave number α may have a spectrum of values, and since N varies with r, we must require

$$\Delta t<2T_{\min} \tag{A4}$$

According to (A3), the smallest values of T correspond to either the largest or the smallest values of α. The largest value of α is $\pi/\Delta z$; with this value, the last term of (A3) dominates. This leads to the usual stability condition for the diffusion equation (providing that also the finite differencing in z is taken into account).

However, we are here concerned with the other case, that α has its smallest value

$$\alpha_{\min}=\frac{\pi}{H} \tag{A5}$$

Then the first term of (A3) dominates; we may ignore the second term and write

$$T_{\min}=\frac{\pi^2 K}{H^2 N^2_{\max}} \tag{A6}$$

According to (59), the largest values of N^2 occur in the central part, where

$$N^2_{\max}=4\Omega_s^2(1+Ro)^2 \tag{A7}$$

From (A4), (A6), and (A7) we finally obtain

$$\Delta t<\frac{2\pi^2K}{H^2N^2_{\max}}=\frac{\pi^2K}{2H^2\Omega_s^2(1+Ro)^2} \tag{A8}$$

which, in non-dimensional form, is the condition (57).

The preceding derivation is slightly faulty in one respect; eq. (A5) would be true if the boundary conditions were, e.g. $v_z^1=0$ at $z=0$ and $z=H$. In reality, however, this condition applies only at $z=H$, whereas at $z=0$ we have $v_z^1=\gamma v'$. This changes the value of $\alpha_{\min}$ a little, but still the condition (A8) appears to be a good approximation. Actually it was found that the stability condition (A8) could be slightly exceeded in some cases, without instability occurring.

REFERENCES

Eliassen, A. 1971. On the Ekman layer in a circular vortex. *J. met. Soc. Japan 49* (Syono Memorial Volume), p. 784.

Greenspan, H. P. & Howard, L. N. 1963. On a time-dependent motion of a rotating fluid. *J. Fluid Mech. 17*, 385.

Greenspan, H. P. 1968. *The Theory of Rotating Fluids.* Cambridge University Press. Cambridge.

Instructions to Authors

GEOPHYSICA NORVEGICA

publishes papers in English. When preparing manuscripts for submission, authors should consult current copies of the journal and follow its style as closely as possible.

MANUSCRIPTS

Manuscript must be typewritten, double spaced throughout, on one side of the paper, with a wide margin. Authors should submit the *original* manuscript (preferably with one copy) to the editor, whose address is shown on page 2 of the cover.

Separate sheets should be used for the following: 1) title page, with the author's name and institution, and, if the title is longer than 40 letters and spaces, a short title not exceeding this limit for use in the running heads; 2) an abstract not exceeding 12 lines (910 letters and spaces) with the name and full postal address underneath of the author to whom communications, proofs, and reprints are to be sent; 3) references; 4) Tables with their headings; 5) legends to Figures.

Brief *Acknowledgements* of grants and other assistance, if any, will be printed at the end of the text.

FIGURES, TABLES, AND MATHEMATICAL SYMBOLS

All illustrations are to be considered as Figures. Each graph, drawing, or photograph should be numbered in sequence with arabic numerals, and should be identified on the back by the name of the journal, the author's name, and the Figure number. The top should be indicated. The Figures should be the original drawing. The columns of *Geophysica Norvegica* are 67 mm broad, and the size of the original drawings should be in proportion. Lines must be thick enough to allow for reduction. Letters and numbers should not be less than 2 mm high in the printed illustration. Photographs should be submitted as unmounted glossy enlargements showing good details.

Tables are to be numbered consecutively. Each Table should be typed on a separate sheet, with a descriptive heading that makes the Table self-explanatory.

All Figures and Tables should be referred to in the text by their number. Their approximate position should be indicated in the margin of the manuscript.

All numbered equations and all unnumbered but complicated equations should be typed on separate lines. Equations should be punctuated.

All text material will be set in roman type unless otherwise marked. Hence, all variables and other characters to be set in italic type should be underlined once with a straight line. Vectors and other characters in boldface type should be indicated by underlining with a single wavy line.

No footnotes should be used.

REFERENCES TO LITERATURE

In the text, Brown (1957, p. 9), Brown & White (1961). If more than two authors, Brown et al. (1963). Multiple references: 'As several authors have reported (Brown 1967, Brown & White 1961, Green et al. 1963)', i. e. chronological order, no commas between names and year.

Lists of References are to be unnumbered and in alphabetical order. The international alphabetical order of Scandinavian and German vowels, should be observed: Å = AA, Æ and Ä = AE, Ø and Ö = OE, Ü = UE. Indicate 1st, 2nd, 3rd, etc. works by the same author in the same year by a, b, c, etc. (White 1966a). No ditto marks should be used. Titles of journals should be abbreviated according to *World List of Scientific Periodicals.*

Examples:

Cadle, R. D. 1966. p. 83 in *Particles in the Atmosphere and Space.* Reinhold Publishing Corporation, New York.

Craig, R. A. 1965. p. 161 in *The Upper Atmosphere. Meteorology and Physics.* International Geophysics Series, Vol. 8. Academic Press, New York and London.

Eliassen, A. & Kleinschmidt, E. 1957. p. 66 in *Handbuch der Physik.* Vol. 48, Part 2, edited by S. Flügge. Springer-Verlag, Berlin.

Junge, C. 1972. *Quart. J. R. Met. Soc. 98,* 711.

PROOFS

Two copies of the first proof will be sent (page proofs). One copy, duly corrected, should be returned to the editor with the least possible delay. All technical parts of the article, including references, names, figures (numbers, formulae), illustrations, etc. are the responsibility of the authors. Authors will be required to pay for any major alterations they may make.

REPRINTS

Fifty reprints of each article will be supplied free. Additional reprints can be ordered at a charge.

International Journals

Title	*Languages*	*Summary/ Abstract*	*Issues per volume*
AMBIO A journal of the Human Environment, Research and Management	English		6
ASTARTE Journal of Arctic Biology	English		2
BLYTTIA Journal of the Norwegian Botanical Association	Norwegian	English	4
BOREAS An International Journal of Quaternary Geology	English, French and German	English	4
LETHAIA An International Journal of Palaeontology and Stratigraphy	English, French and German	English	4
LITHOS An International Journal of Mineralogy, Petrology and Geochemistry	English, French and German	English	4
NORWEGIAN JOURNAL OF ENTOMOLOGY	English, Norwegian and German	English	2
NORSK GEOGRAFISK TIDSSKRIFT Norwegian Journal of Geography	English, Norwegian and German	English	4
NORSK GEOLOGISK TIDSSKRIFT Norwegian Journal of Geology	English, French and German		4
NORWEGIAN JOURNAL OF BOTANY	English, French and German	English	4
ORNIS SCANDINAVICA	English		2

Periodicals

ACTA BOREALIA Journal of Arctic Botany, Geology and Zoology	English
ASTROPHYSICA NORVEGICA Norwegian Journal of Theoretical Astrophysics	English
FOLIA LIMNOLOGICA SCANDINAVICA Scandinavian Journal of Limnology	English
GEOPHYSICA NORVEGICA Geofysiske Publikasjoner	English
SARSIA Journal of Marine Biology	English

UNIVERSITETSFORLAGET

No ISSN 092 551 0072-1174